Voltage-driven Chemical Reactions Enable the Synthesis of Tunable Liquid Ga – Metal Nanoparticles

Valery Okatenko,[†] Coline Boulanger,[†] Alexander N. Chen,[†] Krishna Kumar,[†] Pascal Schouwink,[⊥] Anna Loiudice,[†] Raffaella Buonsanti.[†]*

[†]Laboratory of Nanochemistry for Energy Research, Institute of Chemical Sciences and Engineering, Ecole Politechnique Fédérale de Lausanne, Sion, CH-1950, Switzerland

[⊥]Institute of Chemical Science and Engineering, École Polytechnique Fédérale de Lausanne, Sion, CH-1950, Switzerland

*email: raffaella.buonsanti@epfl.ch

ABSTRACT

Nanosized particles of liquid metals are emerging materials which hold promise for applications spanning from microelectronics to catalysis. Yet, the knowledge of their chemical reactivity is largely unknown. Here, we study the reactivity of liquid Ga and Cu nanoparticles under the application of a cathodic voltage. We discover that the applied voltage and the spatial proximity of these two particle precursors dictate the reaction outcome. In particular, we find that a gradual voltage ramp is crucial to reduce the native oxide skin of the gallium and enable reactive wetting

between the Ga and the Cu nanoparticles; instead, a voltage step causes dewetting between the two. We determine that the use of liquid Ga/Cu nanodimer precursors, which consist of an oxide-covered Ga domain interfaced with a metallic Cu domain, provide a more uniform mixing and result in more homogeneous reaction products compared to a physical mixture of Ga and Cu NPs. Having learned this, we obtain $CuGa_2$ alloys or solid@liquid $CuGa_2$@Ga core@shell nanoparticles by tuning the stoichiometry of the Ga and Cu in the nanodimer precursors. These products reveal an interesting complementarity of thermal and voltage driven synthesis to expand the compositional range of bimetallic NPs. Finally, we extend the voltage-driven synthesis to the combination of Ga with other elements (Ag, Sn, Co, W). By rationalizing the impact of the native skin reduction rate, the wetting properties and the chemical reactivity between Ga and other metals on the results of such voltage-driven chemical manipulation, we define the criteria to predict the outcome of this reaction and set the ground for future studies targeting various applications for multielement nanomaterials based on liquid Ga.

INTRODUCTION

Liquid metals are an emerging class of materials with fascinating properties which result from their dual metallic and liquid nature.[1] These materials provide solutions to a broad set of technology challenges, which include wearable electronics, chemical sensing, and catalysis, both thermal and electro.[2–14] Ga occupies a unique place among the only a few metals with low melting points. Indeed, it is the only metal which is liquid at near-room temperature while being neither toxic nor radioactive, and which does not react violently with air.

In recent years, the importance of Ga-based liquid alloys and solid@liquid nanoparticles (NPs) composed of liquid alloys and solid intermetallics systems has been growing, being these NPs appealing for many of the applications listed above. In addition to minimizing material consumption, the high surface to volume ratio of NPs promotes surface-related phenomena, including surface tension effects, plasmon resonance absorption, surface oxide-induced supercooling and catalysis.[15–26] Especially intriguing is the emerging concept of the Supported Catalytically Active Liquid Metals Solution (SCALMS).[4,27–32] SCALMS are constituted of active metals which are atomically dispersed within a low melting metal matrix; these materials have been exploited especially in thermal catalysis as coke resistant catalysts, being coking one of the most important deactivation mechanisms for high-temperature hydrocarbon chemistry under

reductive conditions.[4,27–32] Despite this growing interest, little is known about the chemistry of liquid metal NPs and their chemical reactivity with other metals.

Existing knowledge indicates that a native oxide skin passivates the Ga surface and hinders its reactivity with other metals.[21,33] In bulk materials, dissolution in basic aqueous solutions and electroreduction of this oxide layer are often utilized to expose the metallic Ga surface and create a metallic contact between Ga and other metals.[34] Once the metallic contact is established, bulk Ga reacts with and corrodes most metals.[35] The reaction might remain confined to the interface between Ga and the second metal, induce a complete transformation into a bimetallic compound,[36] or cause internalization of the second metal within the liquid Ga[37]. The extent of the reaction and the nature of the resulting product determine the property of interest, be it electrical conductivity, mechanical flexibility, surface tension or catalytic selectivity. Furthermore, the chemical reactions between liquid metals and other metals have also an impact on other phenomena, including mechanical degradation, which is relevant for a number of industrial failures.[38] It is therefore important to understand these reactions with more depth. Unfortunately, rational guidelines on how to balance and exploit the chemical reactivity of liquid Ga with other metallic domains to direct the evolution toward a target outcome and thus, regulate their properties, do not exist yet.

Herein, we contribute to fill this knowledge gap by studying the reactivity of liquid Ga NPs with other metallic NPs. We choose the voltage to control the presence of native Ga oxide and, thus, initiate the reaction of the liquid Ga NPs, because of its finer tunability compared to chemical dissolution. We focus on the reaction of Ga with Cu as one exemplificative case because a few reference studies exist on the corresponding bulk materials, which are of interest for creating electrical contacts and antimicrobial coatings as well as driving the electrochemical CO_2 reduction.[36,37,39–45] We use colloidally synthesized Ga and Cu NPs because their size monodispersity and tunability makes them an ideal platform to investigate changes occurring during the reaction and to interrogate the impact of different factors (e.g. relative domain size, stoichiometry, interfaces) on the reaction outcome. We learn that the rate of the applied cathodic voltage is crucial for the reaction to occur. Comparing a physical mixture of Ga and Cu NPs with Ga/Cu nanodimers (NDs), wherein the two NPs share an intimate interface, we demonstrate the importance of spatial proximity and of the relative domain size of the reacting NPs for the reaction outcome, specifically as to whether $CuGa_2$ alloys or unique solid@liquid $CuGa_2$@Ga core@shell NPs form as the reaction product. We also study how the reaction occurs for the bulk materials

under similar conditions and provide the mechanism which links reactivity at the nano and bulk scale. Finally, we extend the learning lesson from Ga – Cu to other metals.

EXPERIMENTAL SECTION

Synthesis of the NP precursors

Liquid Ga/Cu NDs. Liquid Ga/Cu NDs were synthesized according to a previously reported procedure.[21] 2 mL of a solution of pre-synthesized Ga NPs (see **Supplementary Information**) in 1-octadecene (ODE, 4 mM), 2 mL of a solution of $Cu(OAc)_2$ in ODE (4 mM), 1 mL of oleic acid (OLAC) and 1 mL of oleylamine (OLAM) were added to a 5 mL vial and then stirred at 600 rpm on a hot plate at 150 °C inside a glovebox for 6 h ($GaCu_{0.1}$) or 12 h ($GaCu_{0.7}$). Ga/Cu NDs were separated from by-products and from unreacted precursors by adding ethanol (6 mL), followed by centrifugation at 13000 rpm for 10 min. The product was then redispersed in toluene, and the purification/precipitation step was repeated once more before finally being stored in anhydrous toluene (with the final concentration of *ca.* 0.1 mg/mL).

Voltage-driven synthesis

The NP precursors were first deposited on a glassy carbon plate (2.5 cm × 2.5 cm × 0.3 cm, Sigradur G, HTW). Specifically, 15 μg of the NPs in 14 μL of toluene were drop-casted onto a circular area of 1.33 cm^2. After drop-casting, the plates were allowed to dry for 10-15 min, then rinsed with ethanol and with water.

Before deposition, the glassy carbon plates were cleaned by consecutive sonication (Bandelin Sonorex RK 106, 35 kHz) in acetone, isopropanol and water for 10 min each. After this, the glassy carbon plates were polished using an alumina paste (50 nm alumina, BAS Inc.) on a polishing pad. Then, the plates were sonicated in Milli-Q water for another 10 min, polished again on the pad free of alumina to make sure that alumina was removed and, finally, the glassy carbon plate was blown dry.

A Biologic SP-300 was used as a potentiostat. A home-built, custom-made, gas-tight ambient pressure electrochemical H-cell made of polycarbonate and fitted with Buna-N O-rings was used

as the reactor (**Figure S2**). The carbon plates with the deposited NPs (i.e. the working electrode) and counter electrode (Pt foil) were configured parallel to each other to ensure a uniform potential distribution across the surface. Both working and counter electrodes exposed geometric surface areas of 1.33 cm^2 limited by the O-rings. Catholyte and anolyte compartments were each filled with 2 mL electrolyte (0.1 M $KHCO_3$ solution). A Selemion AMV anion exchange membrane was used to separate the anodic and cathodic compartments. Ag/AgCl electrode (leak free series) (Innovative Instruments, Inc.) was used as the reference electrode.

Electrochemical impedance spectroscopy (EIS) was implemented prior to the main chronoamperometry measurement to determine the electrochemical cell resistance (R_{cell}) and compensate for the ohmic losses. Four spectra were measured at the open-circuit potential (ocp), using 41 points between 1 MHz and 100 Hz, using a sinusoidal amplitude of 20 mV and a pause time of 0.6 s between each frequency. Software in-built into the potentiostat software (EC-lab) was used to apply the ohmic loss correction to further measurements.

Materials characterization

Bright-field transmission electron microscopy (TEM) images of the NPs were acquired on a Thermo Fisher Scientific Tecnai-Spirit at 120 kV. 20 µL of as-synthesized NPs were drop-casted on a carbon coated copper TEM grid (Ted Pella, Inc.) to prepare the sample for imaging. To analyze the samples after electrochemistry, a gold or copper TEM grid (Ted Pella, Inc.) was placed on the electrode, 10 µl of ethanol were placed on the area coated with the catalyst, and the catalyst film was gently scratched with the grid.

Selected area electron diffraction (SAED) patterns of the NPs were acquired on a Thermo Fisher Scientific Tecnai-Spirit at 120 kV. To analyze the samples after CO_2RR, the samples were prepared in the way same to described for TEM imaging.

High-angle annular dark field scanning transmission electron microscopy (HAADF-STEM) coupled with energy-dispersive X-ray spectroscopy (EDXS) was performed using a Thermo Fisher Scientific Tecnai Osiris TEM in a scanning mode with an accelerating voltage of 200 kV. The TEM was equipped with a high brightness XFEG gun and four windowless Super-X silicon drift detectors for EDS. Bruker Esprit was used for data analysis.

Grazing incidence X-Ray diffraction (GIXRD) data were collected on a Bruker D8 Discover Plus equipped with a rotating anode (Cu) and a Dectris Eiger2 detector. A focusing 60 mm Göbel mirror was used and the background was optimized with an anti-scatter nozzle and anti-scatter screen. A primary 2.5° axial Soller slit and a secondary 1.0° equatorial Soller slit were placed in the beam path. The incidence angle was optimized on each sample and chosen between 0.1 and 0.25° depending on the sample, the beam was selected using 0.2 or 0.1 mm divergence slits. 2θ scans were collected at stepsizes of 0.5 – 0.6 °2θ and 5 – 10 s per step.

RESULTS AND DISCUSSION

Voltage-driven synthesis of Ga – Cu NPs

We started by investigating the voltage-driven reactivity of a physical mixture of liquid Ga and Cu NPs (**Figures S1**). After depositing the liquid Ga and Cu NPs on glassy carbon plates via drop-casting, we applied a linear voltage scan at 5 mV/s from open circuit potential (ocp) to -0.9 V_{RHE} and held this voltage for 5 minutes as the reaction time in a two-compartments cell (**Figure S2**). The obtained results indicated that the two NPs reacted (**Figure S3**). However, further interpretation of the data was hindered by the intrinsic inhomogeneity of the reaction product resulting from the not uniform distribution of the reactive interfaces in the physical mixture of the NP precursors.

To obtain better control on the spatial distribution of the Cu and Ga domains, we synthesized liquid Ga/Cu nanodimers (NDs), following a previously developed synthesis,[21] and reacted them following the same protocol used for the mixture (**Figure 1A**). The liquid Ga/Cu ND precursors consist of an oxide-covered Ga domain in contact with a metallic Cu domain.[21] We prepared two samples with different domain sizes to investigate the impact of the stoichiometry on the reaction outcome: one with domains of comparable size (~15 and 20 nm, $Ga/Cu_{0.7}$ as determined by elemental analysis) and one with a smaller size of the Cu domain relative to Ga (~7 and 20 nm, $Ga/Cu_{0.1}$ as determined by elemental analysis). The Cu domain is solid and gives diffraction contrast, while the Ga domain is liquid and amorphous in the TEM images of both samples (**Figure 1B,C**).[21]

After reaction, TEM evidences that aggregated NPs with a clear diffraction contrast form from the $Ga/Cu_{0.7}$ NDs (**Figure 1D**); instead, the $Ga/Cu_{0.1}$ NDs transform into better defined NPs each consisting of a smaller solid domain exhibiting diffraction contrast embedded in a larger

amorphous shell (**Figure 1E**). The STEM-EDXS elemental map shows a clear overlap between the Ga and Cu signal for the reaction product of the Ga/$Cu_{0.7}$ NDs (**Figure 1F**), which hints at the formation of an alloy. The overlap of the Ga and Cu signal is noticeable only in the smaller domains of the reaction product of the Ga/$Cu_{0.1}$ NDs, while the larger shell appears to be mostly constituted by Ga (**Figure 1G**). Quantitative analysis of the elemental maps revealed that the Ga/Cu ratio of the NDs is preserved in their final products, which indicates that the reaction goes to completion.

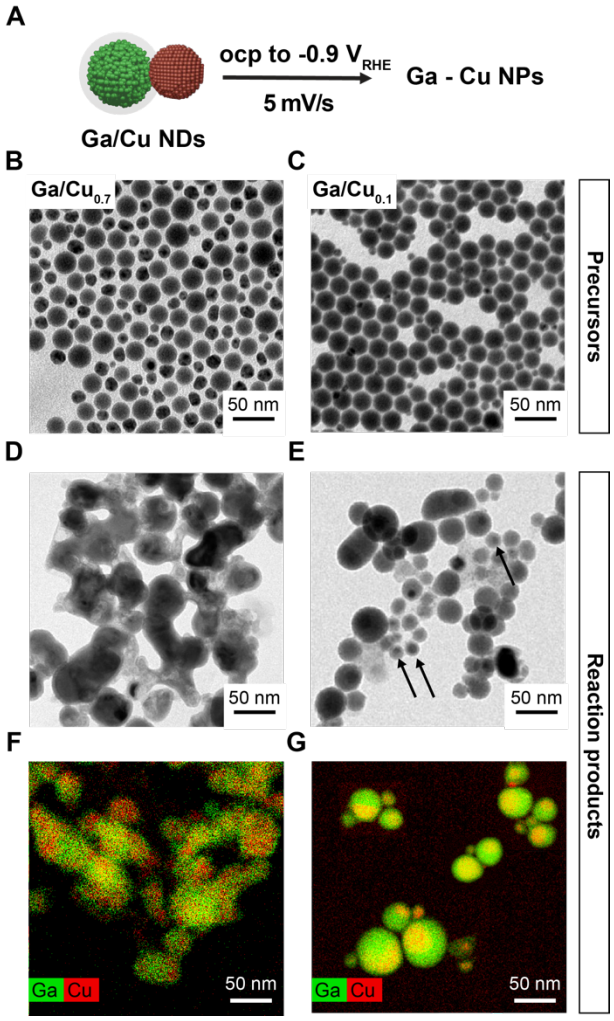

Figure 1. **Voltage-driven reaction of Ga/Cu NDs.** (A) Voltage-driven reaction scheme. (B-E) Bright-field TEM images of (B) Ga/$Cu_{0.7}$ and (C) Ga/$Cu_{0.1}$ NDs with (D,E) the corresponding reaction products NPs. In E, the arrows point at small crystalline domains within

the larger amorphous NPs. (F, G) STEM-EDXS elemental maps (Ga – green, Cu – red) of the reaction products obtained from $Ga/Cu_{0.7}$ (F) and $Ga/Cu_{0.1}$ NDs (G). The reaction was performed by applying a linear voltammetry scan at 5mV/s from ocp to V = -0.9 V_{RHE} with 5 minutes hold as the reaction time. These data evidence that both NDs react and their stoichiometry dictates the reaction outcome.

Intrigued by the differences between the reaction products when the NDs of different stoichiometry are used as precursors, we performed additional structural characterization (**Figure 2**). Electron (SAED, **Figure 2A – C**) and grazing incidence X-Ray diffraction (GIXRD, **Figure 2D**) provided information on the crystal structure. Both analyses propose the existence of the same crystalline phase in the reaction products from both $Ga/Cu_{0.7}$ and $Ga/Cu_{0.1}$ NDs. This phase matches well the $CuGa_2$ intermetallic phase. This observation agrees with reports on bulk liquid Ga – Cu, where reactive wetting results in $CuGa_2$ formation.[36,37,39] The large reflection width in the SAED pattern for the NPs derived from $Ga/Cu_{0.1}$ NDs (**Figure 2C**) originates from small crystallite size (<15 nm), small amount of crystalline phase which is only in the core, and peak overlap due to the relatively low symmetry of $CuGa_2$ phase, which crystallizes in tetragonal *P*4/*mmm* space group.

In addition, we performed HAADF-STEM imaging and STEM-EDXS line profile and elemental mapping on single NPs (**Figure 2E, F**). For the product obtained from $Ga/Cu_{0.7}$ NDs (**Figure 2E**), HAADF-STEM evidences that the product NPs are composed of a uniform core with a thin (*ca.* 2 nm) oxide shell of lower density. The line profile indicates the homogeneous distribution of the Cu and Ga within the NPs, which, along with the overlap of the Cu and Ga signals in the NPs and their atomic composition (66 at. % Ga, 34 at. % Cu), confirms that these NPs are mostly composed of $CuGa_2$ intermetallic. The oxide layer surrounding the NPs most likely forms upon air exposure.[40,41] We will further refer to these NPs as $CuGa_2$ NPs.

In contrast, the line profile of the product obtained from $Ga/Cu_{0.1}$ NDs (**Figure 2F**) indicates that Cu is mostly concentrated in the *ca.* 10 – 15 nm crystalline core while the Ga is more uniformly distributed across the entire NPs. The atomic composition of the core is representative of $CuGa_2$ alloy (66 at. % Ga, 34 at. % Cu). This core is surrounded by a region which is Ga-rich (84 at. % Ga, 16 at. % Cu). Lastly, the NPs are covered with a 2 – 3 nm layer of Ga oxide. As $CuGa_2$ is the only crystalline Ga-containing phase in the sample, the Ga-rich region between the

core and the oxide is amorphous and, most likely, liquid.[18] Thus, we will refer to these NPs as solid@liquid $CuGa_2$@Ga core@shell.

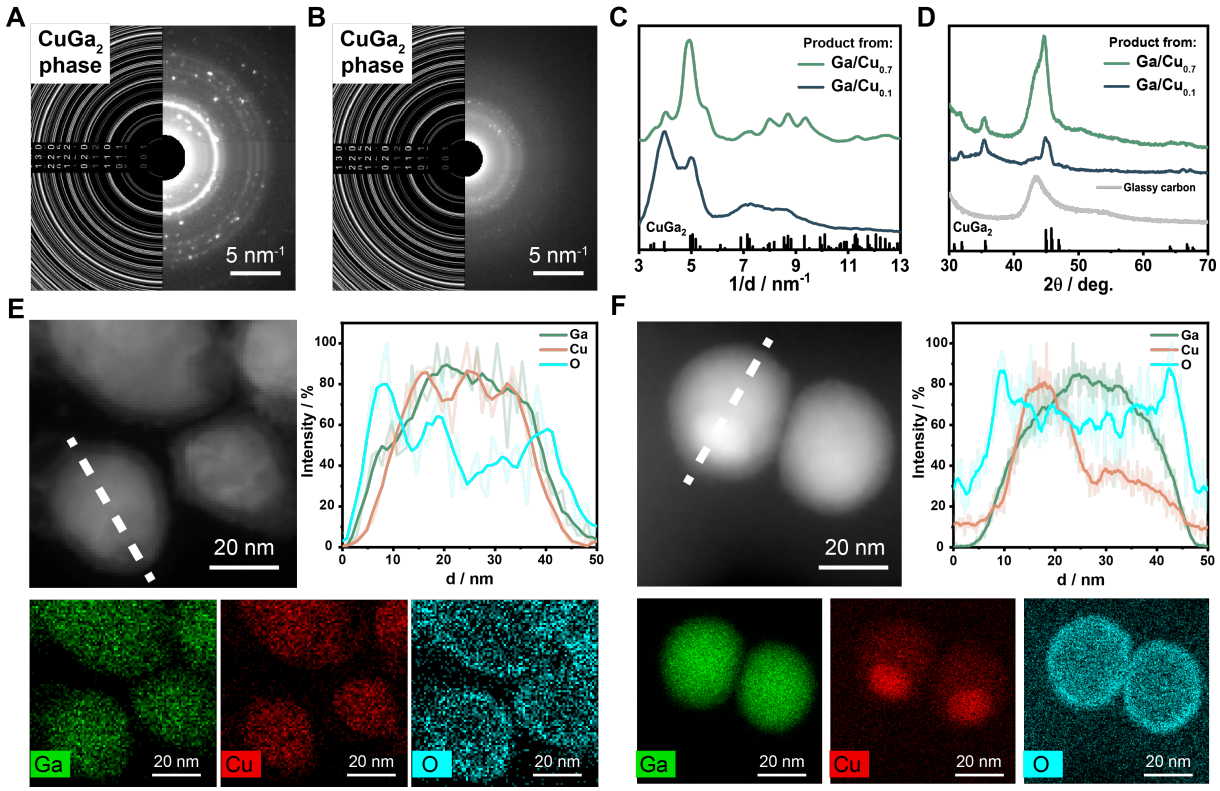

Figure 2. **Structural characterization of Ga – Cu NPs obtained via the voltage-driven synthesis. (A-C)** SAED patterns of the reaction product from (A) $Ga/Cu_{0.7}$ and (B) $Ga/Cu_{0.1}$ NDs and (C) their corresponding circular averaged electron diffraction. (**D**) GIXRD patterns of the reaction products from $Ga/Cu_{0.7}$ and $Ga/Cu_{0.1}$ NDs (the broad reflections at *ca.* 43° and 54° in the arise from the amorphous glassy carbon support). (**E,F**) HAADF-STEM, STEM-EDXS line profiles and elemental maps (Ga – green, Cu – red, O – cyan) of the reaction product from (E) $Ga/Cu_{0.7}$ and (F) $Ga/Cu_{0.1}$ NPs. These data indicate that the $Ga/Cu_{0.7}$ NDs transform into $CuGa_2$ intermetallic NPs while the $Ga/Cu_{0.1}$ NDs yield solid@liquid $CuGa_2$@Ga core@shell NPs.

Influence of synthesis parameters on the reaction outcome

We then varied the reaction time and the voltage to understand the impact of these parameters on the formation of Ga – Cu NPs in the voltage-driven synthesis. We used $Ga/Cu_{0.7}$ NDs as the precursor and collected a voltage series, where we changed the voltage from -0.5 V_{RHE} to -1.1 V_{RHE}

(**Figure 3**). At -0.5 V_{RHE}, no reaction between Cu and Ga occurs and the NDs remain mostly unchanged with separated Cu and Ga domains as seen by HAADF-STEM images and STEM-EDXS elemental maps. The SAED pattern shows no $CuGa_2$ formation, and the main crystalline phase is Cu_2O.

At -0.7 V_{RHE}, HAADF-STEM indicates substantial change of the NDs into bigger NPs. STEM-EDXS evidences mixing of Cu and Ga, although with inhomogeneity in the sample which still contains some unreacted Ga and Cu domains. SAED pattern indicates the presence of $CuGa_2$.

The fact that Cu and Ga in the NDs react at a potential more negative than -0.5 V_{RHE} indicates that the oxide removal is crucial for the reaction to occur between the Cu and Ga NPs. In fact, previous studies on Ga NPs under the same conditions indicated that the Ga oxide skin reduces at -0.54 V_{RHE}.[18]

Sample degradation eventually occurs at -1.1 V_{RHE} which induces Cu fragmentation and coalescence of liquid Ga NPs, consistent with previous studies.[18,46–49]

With this information, we conclude that -0.9 V_{RHE} offers a good balance between providing sufficient driving force for alloy formation without leading to undesired reconstruction of the NPs.

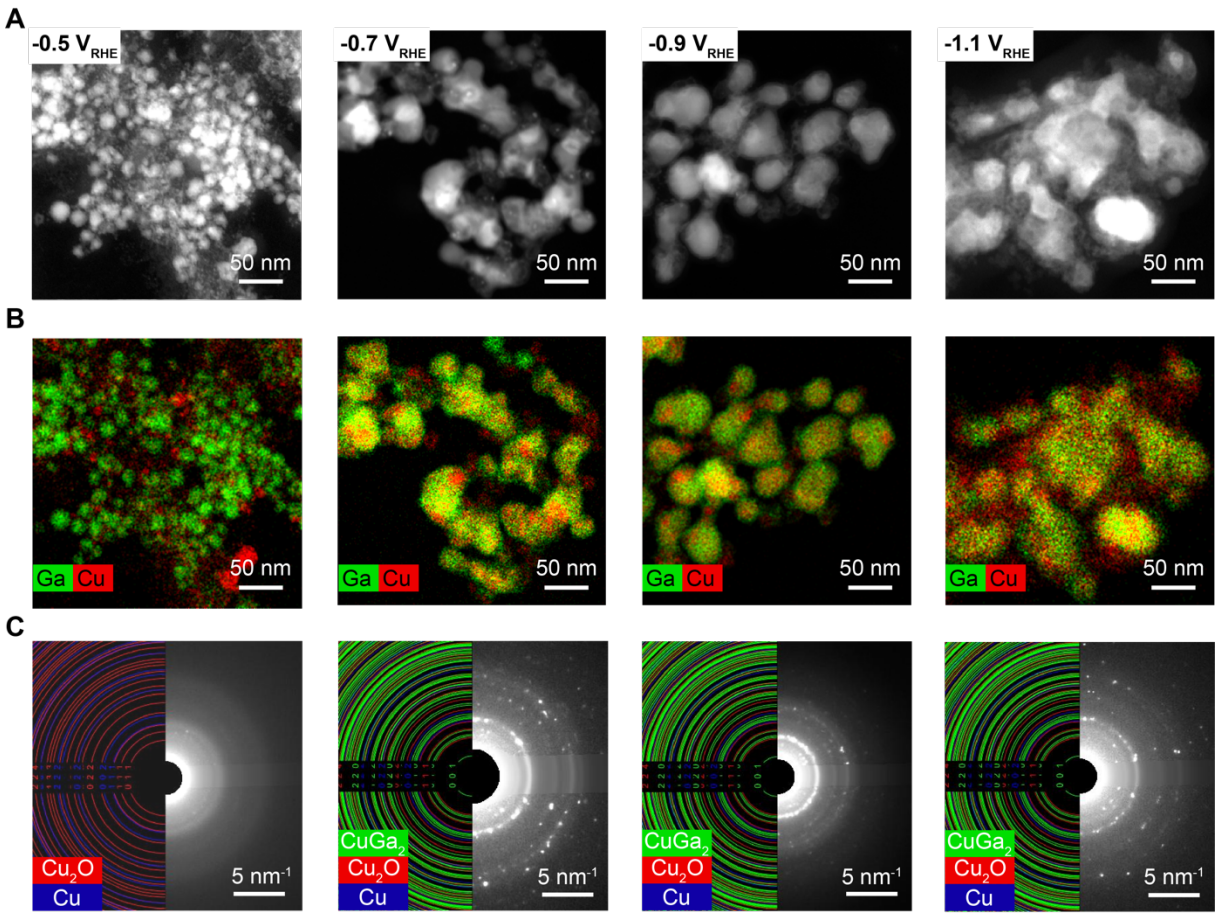

Figure 3. **Voltage-dependence of the voltage-driven synthesis from Ga/$Cu_{0.7}$ NDs as the precursor.** (A) STEM images, (B) STEM-EDXS elemental maps and (C) SAED patterns after voltage scan from ocp to -0.5, -0.7, -0.9 and -1.1 V_{RHE} with 5 min hold as the reaction time. These data indicate that an optimal voltage exists to controllably form the Ga – Cu NPs; this voltage reduces the Ga native skin without driving the reconstruction of the Ga – Cu NPs which form as the reaction product.

In a complementary set of experiments, we fixed the voltage at -0.9 V_{RHE} and varied the reaction time from 1 minute to 60 minutes (**Figure 4**). HAADF-STEM image indicates substantial change of the NDs into larger NPs already after 1 minute; however, the STEM-EDXS elemental maps and SAED patterns suggest that the reaction is not complete yet after this time. Indeed, Cu and Ga are mostly separated, as in the NDs used as precursors, and the diffraction signal is relatively weak. During this early reaction time, the reaction is probably still confined at the interface only.

As time passes and the reaction progresses, HAADF-STEM images do not show substantial change, however the STEM-EDXS maps indicate a spatially homogeneous distribution of the Cu and Ga signal while the $CuGa_2$ diffraction signal in the SAED becomes more intense. The samples at 5 and 30 minutes are quite similar to each other. Instead, segregation between the Cu and Ga occurs after 60 minutes, as indicated by the STEM-EDXS maps, with the SAED pattern suggesting the dominance of crystalline Cu_2O in the sample.

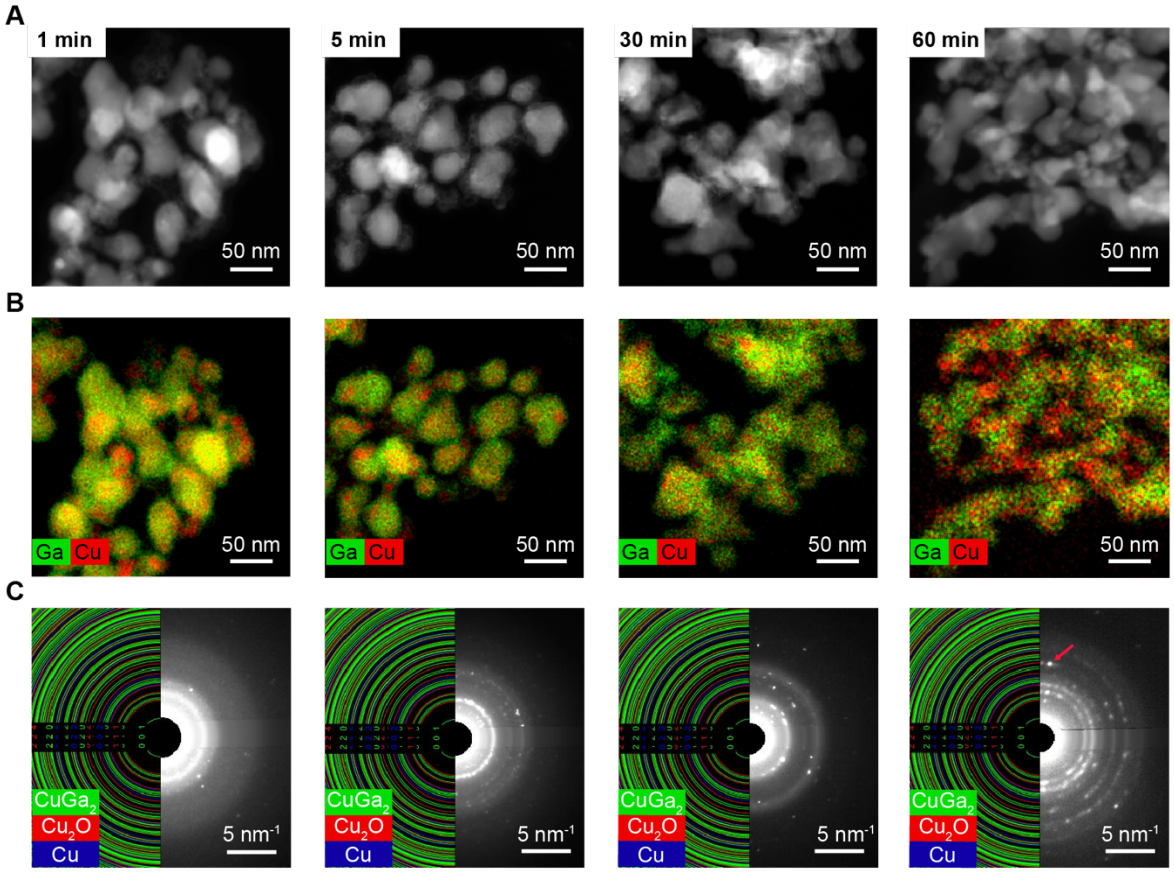

Figure 4. **Time-dependence of the voltage-driven synthesis from Ga/$Cu_{0.7}$ NDs as the precursor.** (A) STEM images, (B) STEM-EDXS elemental maps and (C) SAED patterns after voltage scan from ocp to -0.9 V_{RHE} with 1, 5, 30 and 60 minutes hold as the reaction time. $CuGa_2$ is the main crystalline phase at 5 and 30 minutes, instead Cu_2O dominates at 60 minutes (the (022) diffraction spot is marked by red arrow for clarity). These data indicate that the reaction reaches completion at 5 minutes while phase segregation takes place for reaction time ≥ 60 minutes.

Lastly, we evaluated the impact of the voltage scan rate on the reaction outcome. Interestingly, the application of a voltage step instead of a voltage scan makes Ga disappear from the substrate, with less Ga being detected at more negative voltage (**Figure S4**). $CuGa_2$ does not form in this scenario.

To better understand how the Ga loss takes place, we complemented these tests with studies on bulk liquid Ga – Cu samples, which consisted of a Ga droplet deposited on a Cu foil (**Supplementary Videos S1 – S5, Figures S5, S6**). Here, we made observations similar to those made on the NDs. The Ga drop remains on Cu surface, eventually wets it and forms $CuGa_2$ intermetallic at the interface (**Supplementary Video S1, Figure S5A**) when the voltage is applied at 5 mV/s.[36,37] On the contrary, the Ga droplet quickly escapes from the Cu foil surface (**Supplementary Video S2, Figure S5B**) or from the surface of the inert glassy carbon support (**Supplementary Video S3, Figure S5C**) upon the application of a voltage step. We observed the same behavior for a bulk "dimer" structure which mimics the liquid Ga/Cu NDs, where only a 5 mV/s scan enables Cu and Ga to react and form a $CuGa_2$ interface (**Supplementary Videos S4, S5, Figure S6**).

Mechanism of the voltage-driven reaction between Ga and Cu

With the evidence provided by the compositional and structural analyses and the study of the synthesis parameters discussed above, a complete picture of the reaction mechanism shapes up (**Figure 5**).

As a reminder, the liquid Ga/Cu ND precursors are described as an oxide-covered Ga domain in contact with a metallic Cu domain. The abrupt application of a cathodic voltage, which is sufficient to reduce the Ga oxide skin (< -0.54 V_{RHE}), induces a sudden increase in surface tension of the liquid Ga domain, while Cu domain remains static. Ga does not wet Cu.[36] Thus, Ga escapes from Cu. A similar effect was observed by Mayyas et al.[50] Here, the authors showed that In can be expelled from an eutectic GaIn melt in the form of NPs by applying voltage pulses of large magnitude. Jumping of liquid metal droplets resulting from a drastic change of surface tension between the metallic and oxidized state induced by a potential step has also been reported, which relates to the observation made in this work.[51] Eventually, electrostatic repulsion between Ga and Cu might also be involved in addition to change in surface tension.

The repulsion between Cu and Ga can be overturned by decreasing the reduction rate of the oxide skin to allow sufficient time for the intermetallic to form, which eventually changes the wetting behavior. We achieved such balance by tuning the rate of the applied voltage and found 5 mV/s to be an optimal rate. Once the $CuGa_2$ interface forms, reactive wetting takes place, and the reaction proceeds further towards the bulk of the NPs. While a similar process may occur in the physical mixture of Cu and liquid Ga NPs (**Figure S3**), the NDs provide more uniform mixing of the Cu and Ga domains, which largely improves the uniformity of resulting intermetallic NPs.

As reactive wetting takes place, the stoichiometry of the two reagents Cu and Ga in the ND precursors determines the outcome product. For Ga:Cu < 2:1 (i.e. $Ga/Cu_{0.7}$ NDs), the reaction goes to completion and $CuGa_2$ forms almost uniquely. Differently, for Ga:Cu > 2:1 (i.e. $Ga/Cu_{0.1}$ NDs), the excess Ga wets the $CuGa_2$ surface, resulting in a peculiar process described as wetting-assisted internalization of a solid NP in the liquid Ga NP, and yielding a solid $CuGa_2$ core floating inside the liquid metal Ga host NP, similarly to a phenomenon previously observed in Cu-In microparticles.[16] Liquid Ga, in its turn, remains covered by a non-passivating Ga oxide skin, which keeps the NPs separate and hinders their coalescence. This observation suggests that the non-passivating oxide skin is probably of transient nature, and is constantly formed and reduced at cathodic voltage, rather than remaining as a static residual skin, which is in line with our previous study.[18] Indeed, a static skin would not allow the pure metallic contact of liquid Ga with Cu domain accompanied by the formation of $CuGa_2$ intermetallic.

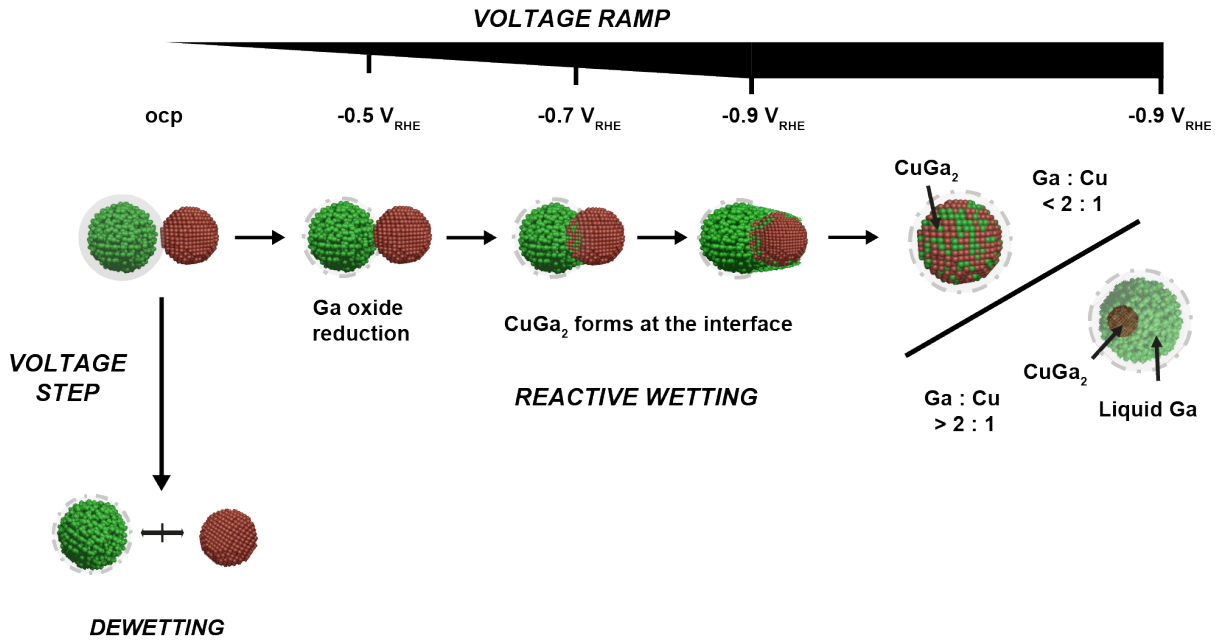

Figure 5. Schematic of the voltage-driven reaction of liquid Ga/Cu NDs.

Lastly, we hypothesize that the more Cu-rich phases than $CuGa_2$ in the Ga-Cu phase diagram (Cu_9Ga_4 and the Cu *fcc*-based solid solution of Ga in Cu) do not form because of the high activation barrier which the transformation from the $CuGa_2$ structure to these other phases requires. Interestingly, we have approached the opposite limitation in our previous study where we used a seeded-growth amalgamation reaction in solution to form Ga – Cu alloyed NCs using heat as the driving force for reactivity.[41] Here, starting from a Cu NP seed and injecting a Ga molecular precursor, we obtained the Cu-rich phases of the Ga – Cu phase diagram, but any phase more Ga-rich than Cu_9Ga_4-type phase (such as $CuGa_2$) was not accessible. With this study, we obtain this missing Ga – Cu intermetallic composition and expand the Ga – Cu NP library demonstrating the complementarity of synthetic approaches exploiting different driving forces.

Generality of the voltage-driven liquid Ga reactivity at the nanoscale

Chemical reactivity (*i.e.,* reactivity driven by the formation of stable bimetallic compounds) and wetting are both in place for the Ga – Cu system. To understand if and how the voltage-driven synthesis can be extended to form other Ga-based NPs, we tested the synthesis with other metals. We chose Ag, Co, W and Sn as other elements to react with Ga based on the following reasoning.

Ag and Co are both transition metals which form intermetallic compounds with Ga based on bulk phase diagrams. However, Ag is reactively wetted by Ga, while Co may not be, based on its vicinity to Ni for which a previous study exist.[37] W is a transition metal which does not chemically react with Ga in the bulk at ambient conditions.[35] Sn is an example of post-transition metal, for which no intermetallic formation is reported.[52] To the best of our knowledge, no information on the wettability of W and Sn by Ga has been reported. By evaluating how the reaction between Ga and Ag, Co, W and Sn proceeds, we aimed to establish the primary design rules for the formation of Ga-based NPs with other metals among the Periodic Table, where we targeted transition (Ag, Co, W) and post-transition (Sn) metals which normally do (Ag, Co) and do not (W, Sn) react with Ga, potentially with a different wetting behavior between Ag and Co.

With this in mind, we synthesized Ga/M NDs (M = Ag, Co, Sn) and prepared physical mixture of Ga with WO_3 NPs of overall $Ga(WO_3)_{0.1}$ composition (**Figure S7**). We reacted them under the same optimal conditions found for the Ga – Cu (*i.e.,* 5mV/s ramp from ocp to -0.9 V_{RHE} and 5 min reaction time at this voltage). **Figure 6** summarizes the obtained results.

$Ga/Ag_{0.3}$ NDs react to form new NPs including smaller NPs with diffraction contrast embedded into larger amorphous NPs (**Figure 6A**). STEM-EDXS evidences the presence of Ag and Ga in the smaller NPs and Ga only in the larger domain (**Figure 6E**). SAED indicates that the crystalline domains internalized in the Ga are Ag_2Ga (**Figure 6I**). Overall, Ag react similarly to Cu, consistently with its wettability by Ga and chemical reactivity.[37]

Interestingly, $Ga/(CoO)_{0.1}$ NDs do not react despite the phase diagram showing that stable intermetallic compounds are formed between Ga and Co. Indeed, both TEM (**Figure 6B**) and STEM-EDXS (**Figure 6F**) are consistent with the dimer-like configuration of the starting precursor (**Figure S6**) and the SAED (**Figure 6J**) indicates only crystalline cobalt oxide. This result is similar to the finding of an earlier report wherein the internalization of Ni into a bulk Ga drop was not successful.[37] The presence of an oxide layer might explain the non-wetting of the Ga towards Ni and Co. The Pourbaix diagram makes the existence of CoO improbable during the reaction, as CoO supposedly reduces to metallic Co at more positive voltages than Ga (0.1 *vs.* -0.5 V_{RHE}, respectively).[53] Yet, a layer of oxide might still exist as previously observed for Ga NPs under similar conditions.[18] Alternatively, non-wetting of metallic Co with Ga may justify the absence of reaction and internalization of Co into Ga, although data supporting this hypothesis do not exist at this moment.

The physical mixture of liquid Ga NPs and WO_3 NPs react to form a new material, based on TEM images, which is different compared to the starting NPs (**Figure 6C, Figure S6**). The W signal in STEM-EDXS spectrum is above the detection limit in the Ga – W NPs after the reaction, yet the intensity is too low to localize it in a particular part of the new NPs (**Figure 6D**). The SAED (**Figure 6E**) suggests the formation of Ga_5W_2 as minor reaction product, an intermetallic compound which is reported to exist at elevated pressures[54]. While SAED is not conclusive because of the weak diffraction signal, this result indicates that new reactivities might emerge at the nanoscale.

Lastly, TEM image proposes the presence of a solid particle in Ga (**Figure 6D**) as a result of the voltage-driven reaction of $Ga/Sn_{0.1}$ NDs. However, STEM-EDXS elemental mapping shows no reliable Sn signal (**Figure 6H**). Yet, SAED suggests that crystalline domains do form (**Figure 6L**). While acknowledging the limited information that this diffraction pattern provides for low-symmetry phases, the signal matches δ-Ga, which has been reported to be a stable crystalline phase in the Ga NPs.[18,20] The Ga and Sn phase diagram does not suggest intermetallic formation.[52] Thus, we speculatively attribute this result to Ga doping with Sn, facilitating partial Ga solidification.

Altogether, the reactivity studies of Ga/Ag, Ga/(CoO), Ga-$(WO_3)_{0.1}$ and Ga/Sn along with that of the Ga/Cu indicate that wetting and chemical reactivity are good indicators for a successful voltage-driven synthesis of Ga-based NPs. At the same time, new reactivities might still emerge at the nanoscale which deviate from this golden rule and are worth exploring. With the assumption that other metal NPs can be reactively wetted by Ga, we believe our observations indicate the possibility to extend the scope of reactive wetting to synthesize a larger library of bimetallic Ga-based NPs.

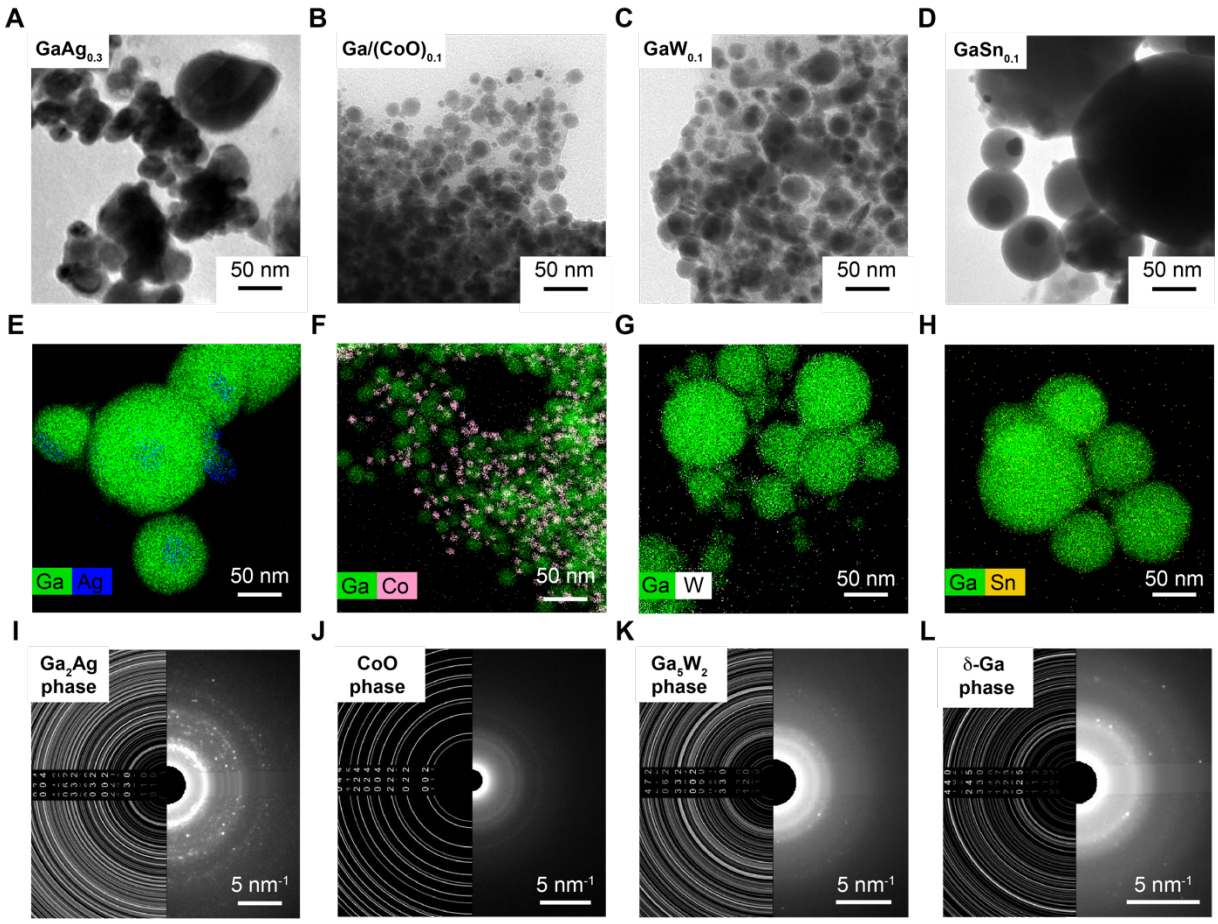

Figure 6. Extension of the voltage-driven synthesis to different Ga-M systems. (A – D) TEM images, (E – H) STEM-EDXS elemental maps and (I – K) SAED patterns of the reaction products obtained from (A, E, I) $Ga/Ag_{0.3}$ NDs, (B, F, J) $Ga/(CoO)_{0.1}$ NDs, (C, G, K) physical mixture of Ga and WO_3 NPs and (D, H, L) $GaSn_{0.1}$. These data indicate that both wettability and chemical reactivity are important in determining the reaction outcome.

CONCLUSIONS

In this study, we explored the chemical reactivity of liquid Ga NPs with other metal NPs driven by an applied voltage. We demonstrated that the rate of such voltage, which controls the reduction rate of the native Ga oxide skin, along with the wetting properties between elements and their chemical reactivities, enables the reactive wetting of liquid Ga NPs and the formation of bimetallic Ga-based NPs.

We discovered that $CuGa_2$ alloyed NPs and solid@liquid core@shell NPs, where a $CuGa_2$ nanocrystal floats inside a liquid Ga NP, can be obtained from liquid Ga/Cu NDs, which we used as a case study, by tuning the initial stoichiometry of Ga and Cu. While the same approach applies to the physical mixture of Cu and Ga NPs, the NDs ensure more uniform mixing on the NP precursors. The formation of Ga-rich alloys points at the complementarity of the thermal and voltage driven synthesis to expand the compositional range of bimetallic NPs. The solid@liquid NPs are unique and only a few other examples exist in the literature, although not with the same degree of sample homogeneity obtained herein.[15,16,55]

Finally, we proved that this approach can be extended to the combination of Ga with other elements (Ag, Co, W, Sn).

By presenting a rational framework which explains the formation of bimetallic NPs via the proposed voltage-driven synthesis, we believe this report sets the ground for future studies targeting various applications for multimetallic Ga-based NPs, including those with a liquid Ga domain.

ASSOCIATED CONTENT

The Supporting Information is available and free of charge and contains additional experimental and characterization details, TEM, STEM, STEM-EDXS, SAED, movies.

NOTES

The authors declare no competing financial interest.

ACKNOWLEDGMENTS

This work was equally supported by the Swiss National Science Foundation (SNSF) under grant number 200021L_191997/1 and by the Swiss State Secretariat for Education, Research and Innovation (SERI) Horizon Europe under contract number 589014.

REFERENCES

(1) Tang, S. Y.; Tabor, C.; Kalantar-Zadeh, K.; Dickey, M. D. Gallium Liquid Metal: The Devil's Elixir. *Annu. Rev. Mater. Res.* **2021**, *51*, 381–408.

(2) Daeneke, T.; Khoshmanesh, K.; Mahmood, N.; De Castro, I. A.; Esrafilzadeh, D.; Barrow, S. J.; Dickey, M. D.; Kalantar-Zadeh, K. Liquid Metals: Fundamentals and Applications in Chemistry. *Chem. Soc. Rev.* **2018**, *47*, 4073–4111.

(3) Dickey, M. D. Emerging Applications of Liquid Metals Featuring Surface Oxides. *ACS Appl. Mater. Interfaces* **2014**, *6*, 18369–18379.

(4) Rahim, M. A.; Tang, J.; Christofferson, A. J.; Kumar, P. V.; Meftahi, N.; Centurion, F.; Cao, Z.; Tang, J.; Baharfar, M.; Mayyas, M.; Allioux, F. M.; Koshy, P.; Daeneke, T.; McConville, C. F.; Kaner, R. B.; Russo, S. P.; Kalantar-Zadeh, K. Low-Temperature Liquid Platinum Catalyst. *Nat. Chem.* **2022**, *14*, 935–941.

(5) Hou, Y.; Wang, F.; Qin, C.; Wu, S.; Cao, M.; Yang, P.; Huang, L.; Wu, Y. A Self-Healing Electrocatalytic System via Electrohydrodynamics Induced Evolution in Liquid Metal. *Nat. Commun.* **2022**, *13*, 7625.

(6) Wang, X.; Yao, W.; Guo, R.; Yang, X.; Tang, J.; Zhang, J.; Gao, W.; Timchenko, V.; Liu, J. Soft and Moldable Mg-Doped Liquid Metal for Conformable Skin Tumor Photothermal Therapy. *Adv. Healthc. Mater.* **2018**, *7*, 1800318.

(7) Etienne Palleau, C.; Reece, S.; Desai, S. C.; Smith, M. E.; Dickey, M. D.; Palleau, E.; Reece, S.; Desai, S. C.; Dickey, M. D.; Smith, M. E. Self-Healing Stretchable Wires for Reconfigurable Circuit Wiring and 3D Microfluidics. *Adv. Mater.* **2013**, *25*, 1589–1592.

(8) Lu, Y.; Hu, Q.; Lin, Y.; Pacardo, D. B.; Wang, C.; Sun, W.; Ligler, F. S.; Dickey, M. D.; Gu, Z. Transformable Liquid-Metal Nanomedicine. *Nat. Commun.* **2015**, *6*, 10066.

(9) Esrafilzadeh, D.; Zavabeti, A.; Jalili, R.; Atkin, P.; Choi, J.; Carey, B. J.; Brkljača, R.; O'Mullane, A. P.; Dickey, M. D.; Officer, D. L.; MacFarlane, D. R.; Daeneke, T.; Kalantar-Zadeh, K. Room Temperature CO_2 Reduction to Solid Carbon Species on Liquid Metals Featuring Atomically Thin Ceria Interfaces. *Nat. Commun.* **2019**, *10*, 865.

(10) He, Y.; Tang, J.; Kalantar-Zadeh, K.; Dickey, M. D.; Wang, X. Noncontact Rotation, Levitation, and Acceleration of Flowing Liquid Metal Wires. *Proc. Natl. Acad. Sci. U. S. A.* **2022**, *119*, e2117535119.

(11) Lin, Y.; Cooper, C.; Wang, M.; Adams, J. J.; Genzer, J.; Dickey, M. D. Handwritten, Soft

Circuit Boards and Antennas Using Liquid Metal Nanoparticles. *Small* **2015**, *11*, 6397–6403.

(12) Ye, L.; Syed, N.; Wang, D.; Guo, J.; Yang, J.; Buston, J.; Singh, R.; Alivand, M. S.; Kevin Li, G.; Zavabeti, A. Low-Temperature CO_2 Reduction Using Mg–Ga Liquid Metal Interface. *Adv. Mater. Interfaces* **2023**, *10*, 2201625.

(13) Upham, D. C.; Agarwal, V.; Khechfe, A.; Snodgrass, Z. R.; Gordon, M. J.; Metiu, H.; McFarland, E. W. Catalytic Molten Metals for the Direct Conversion of Methane to Hydrogen and Separable Carbon. *Science* **2017**, *358*, 917–921.

(14) Crawford, J.; Yin, H.; Du, A.; O'Mullane, A. P. Nitrate-to-Ammonia Conversion at an InSn-Enriched Liquid-Metal Electrode. *Angew. Chem., Int. Ed.* **2022**, *61*, e202201604.

(15) O'Mullane, A. Realizing Solid Core/Liquid Shell Nanomaterials at Room Temperature. *Matter* **2019**, *1*, 22–23.

(16) Tang, S. Y.; Mitchell, D. R. G.; Zhao, Q.; Yuan, D.; Yun, G.; Zhang, Y.; Qiao, R.; Lin, Y.; Dickey, M. D.; Li, W. Phase Separation in Liquid Metal Nanoparticles. *Matter* **2019**, *1*, 192–204.

(17) Martin, A.; Chang, B. S.; Pauls, A. M.; Du, C.; Thuo, M. Stabilization of Undercooled Metals via Passivating Oxide Layers. *Angew. Chem., Int. Ed.* **2021**, *60*, 5928–5935.

(18) Okatenko, V.; Castilla-Amorós, L.; Stoian, D. C.; Vávra, J.; Loiudice, A.; Buonsanti, R. The Native Oxide Skin of Liquid Metal Ga Nanoparticles Prevents Their Rapid Coalescence during Electrocatalysis. *J. Am. Chem. Soc.* **2022**, *144*, 10053–10063.

(19) Losurdo, M.; Suvorova, A.; Rubanov, S.; Hingerl, K.; Brown, A. S. Thermally Stable Coexistence of Liquid and Solid Phases in Gallium Nanoparticles. *Nat. Mater.* **2016**, *15*, 995–1002.

(20) Yarema, M.; Wörle, M.; Rossell, M. D.; Erni, R.; Caputo, R.; Protesescu, L.; Kravchyk, K. V.; Dirin, D. N.; Lienau, K.; Von Rohr, F.; Schilling, A.; Nachtegaal, M.; Kovalenko, M. V. Monodisperse Colloidal Gallium Nanoparticles: Synthesis, Low Temperature Crystallization, Surface Plasmon Resonance and Li-Ion Storage. *J. Am. Chem. Soc.* **2014**, *136*, 12422–12430.

(21) Castilla-Amoros, L.; Stoian, D.; Pankhurst, J.; Varandili, S.; Buonsanti, R. Exploring the Chemical Reactivity of Gallium Liquid Metal Nanoparticles in Galvanic Replacement. *J. Am. Chem. Soc.* **2020**, *142*, 19283–19290.

(22) Castilla-Amorós, L.; Chien, T. C. C.; Pankhurst, J. R.; Buonsanti, R. Modulating the Reactivity of Liquid Ga Nanoparticle Inks by Modifying Their Surface Chemistry. *J. Am. Chem. Soc.* **2022**, *144*, 1993–2001.

(23) Idrus-Saidi, S. A.; Tang, J.; Ghasemian, M. B.; Yang, J.; Han, J.; Syed, N.; Daeneke, T.; Abbasi, R.; Koshy, P.; O'Mullane, A. P.; Kalantar-Zadeh, K. Liquid Metal Core–Shell Structures Functionalised via Mechanical Agitation: The Example of Field's Metal. *J. Mater. Chem. A* **2019**, *7*, 17876–17887.

(24) Ghigna, P.; Spinolo, G.; Parravicini, G. B.; Stella, A.; Migliori, A.; Kofman, R. Metallic versus Covalent Bonding: Ga Nanoparticles as a Case Study. *J. Am. Chem. Soc.* **2007**, *129*, 8026–8033.

(25) Martin, A.; Kiarie, W.; Chang, B.; Thuo, M. Chameleon Metals: Autonomous Nano-Texturing and Composition Inversion on Liquid Metals Surfaces. *Angew. Chemie* **2020**, *132*, 360–365.

(26) Zavabeti, A.; Ou, J. Z.; Carey, B. J.; Syed, N.; Orrell-Trigg, R.; Mayes, E. L. H.; Xu, C.; Kavehei, O.; O'Mullane, A. P.; Kaner, R. B.; Kalantar-Zadeh, K.; Daeneke, T. A Liquid Metal Reaction Environment for the Room-Temperature Synthesis of Atomically Thin Metal Oxides. *Science* **2017**, *358*, 332–335.

(27) Taccardi, N.; Grabau, M.; Debuschewitz, J.; Distaso, M.; Brandl, M.; Hock, R.; Maier, F.; Papp, C.; Erhard, J.; Neiss, C.; Peukert, W.; Görling, A.; Steinrück, H. P.; Wasserscheid, P. Gallium-Rich Pd–Ga Phases as Supported Liquid Metal Catalysts. *Nat. Chem.* **2017**, *9*, 862–867.

(28) Raman, N.; Maisel, S.; Grabau, M.; Taccardi, N.; Debuschewitz, J.; Wolf, M.; Wittkämper, H.; Bauer, T.; Wu, M.; Haumann, M.; Papp, C.; Görling, A.; Spiecker, E.; Libuda, J.; Steinrück, H. P.; Wasserscheid, P. Highly Effective Propane Dehydrogenation Using Ga-Rh Supported Catalytically Active Liquid Metal Solutions. *ACS Catal.* **2019**, *9*, 9499–9507.

(29) Wirth, J.; Englisch, S.; Drobek, D.; Apeleo Zubiri, B.; Wu, M.; Taccardi, N.; Raman, N.; Wasserscheid, P.; Spiecker, E. Unraveling Structural Details in Ga-Pd SCALMS Systems Using Correlative Nano-CT, 360° Electron Tomography and Analytical TEM. *Catal.* **2021**, *11*, 810.

(30) Søgaard, A.; De Oliveira, A. L.; Taccardi, N.; Haumann, M.; Wasserscheid, P. Ga–Ni Supported Catalytically Active Liquid Metal Solutions (SCALMS) for Selective Ethylene

Oligomerization. *Catal. Sci. Technol.* **2021**, *11*, 7535–7539.

(31) Wittkämper, H.; Hock, R.; Weißer, M.; Dallmann, J.; Vogel, C.; Raman, N.; Tacardi, N.; Haumann, M.; Wasserscheid, P.; Hsieh, T. E.; Maisel, S.; Moritz, M.; Wichmann, C.; Frisch, J.; Gorgoi, M.; Wilks, R. G.; Bär, M.; Wu, M.; Spiecker, E.; Görling, A.; Unruh, T.; Steinrück, H. P.; Papp, C. Isolated Rh Atoms in Dehydrogenation Catalysis. *Sci. Rep.* **2023**, *13*, 4458.

(32) Raman, N.; Söllner, J.; Madubuko, N.; Nair, S.; Taccardi, N.; Thommes, M.; Haumann, M.; Wasserscheid, P. Top-down vs. Bottom-up Synthesis of Ga–Based Supported Catalytically Active Liquid Metal Solutions (SCALMS) for the Dehydrogenation of Isobutane. *Chem. Eng. J.* **2023**, *475*, 146081.

(33) Martin, A.; Du, C.; Chang, B.; Thuo, M. Complexity and Opportunities in Liquid Metal Surface Oxides. *Chem. Mater.* **2020**, *32*, 9045–9055.

(34) Khan, M. R.; Eaker, C. B.; Bowden, E. F.; Dickey, M. D. Giant and Switchable Surface Activity of Liquid Metal via Surface Oxidation. *Proc. Natl. Acad. Sci. U. S. A.* **2014**, *111*, 14047–14051.

(35) Lyon, R. N. *Liquid-Metals Handbook*, 1st ed.; Lyon, R. N., Ed.; U.S. Government Printing Office: Washington, D.C., 1954.

(36) Ma, J. L.; Dong, H. X.; He, Z. Z. Electrochemically Enabled Manipulation of Gallium-Based Liquid Metals within Porous Copper. *Mater. Horizons* **2018**, *5*, 675–682.

(37) Tang, J.; Zhao, X.; Li, J.; Zhou, Y.; Liu, J.; Tang, J.; Liu, J.; Zhao, X.; Zhou, Y.; Li, J. Liquid Metal Phagocytosis: Intermetallic Wetting Induced Particle Internalization. *Adv. Sci.* **2017**, *4*, 1700024.

(38) Norkett, J. E.; Dickey, M. D.; Miller, V. M. A Review of Liquid Metal Embrittlement: Cracking Open the Disparate Mechanisms. *Metall. Mater. Trans. A Phys. Metall. Mater. Sci.* **2021**, *52*, 2158–2172.

(39) Kwon, K. Y.; Cheeseman, S.; Frias-De-Diego, A.; Hong, H.; Yang, J.; Jung, W.; Yin, H.; Murdoch, B. J.; Scholle, F.; Crook, N.; Crisci, E.; Dickey, M. D.; Truong, V. K.; Kim, T. A Liquid Metal Mediated Metallic Coating for Antimicrobial and Antiviral Fabrics. *Adv. Mater.* **2021**, *33*, 2104298.

(40) Bagchi, D.; Raj, J.; Kumar Singh, A.; Cherevotan, A.; Roy, S.; Manoj, K. S.; Vinod, C. P.; Peter, S. C. Structure-Tailored Surface Oxide on Cu-Ga Intermetallics Enhances CO_2

Reduction Selectivity to Methanol at Ultra-Low Potential. *Adv. Mater.* **2022**, 2109426.

(41) Okatenko, V.; Loiudice, A.; Newton, M. A.; Stoian, D. C.; Blokhina, A.; Chen, A. N.; Rossi, K.; Buonsanti, R. Alloying as a Strategy to Boost the Stability of Copper Nanocatalysts during the Electrochemical CO_2 Reduction Reaction. *J. Am. Chem. Soc.* **2023**, *145*, 5370–5383.

(42) Dickey, M. D. Stretchable and Soft Electronics Using Liquid Metals. *Adv. Mater.* **2017**, *29*, 1606425.

(43) Erlenbach, S.; Mondal, K.; Ma, J.; Neumann, T. V.; Ma, S.; Holbery, J. D.; Dickey, M. D. Flexible-to-Stretchable Mechanical and Electrical Interconnects. *ACS Appl. Mater. Interfaces* **2023**, *15*, 6005–6012.

(44) Sato, T.; Yamagishi, K.; Hashimoto, M.; Iwase, E. Method to Reduce the Contact Resistivity between Galinstan and a Copper Electrode for Electrical Connection in Flexible Devices. *ACS Appl. Mater. Interfaces* **2021**, *13*, 18247–18254.

(45) Zhu, S.; So, J. H.; Mays, R.; Desai, S.; Barnes, W. R.; Pourdeyhimi, B.; Dickey, M. D. Ultrastretchable Fibers with Metallic Conductivity Using a Liquid Metal Alloy Core. *Adv. Funct. Mater.* **2013**, *23*, 2308–2314.

(46) Popović, S.; Smiljanić, M.; Jovanovič, P.; Vavra, J.; Buonsanti, R.; Hodnik, N. Stability and Degradation Mechanisms of Copper-Based Catalysts for Electrochemical CO_2 Reduction. *Angew. Chem., Int. Ed.* **2020**, *59*, 14736–14746.

(47) Huang, J.; Hörmann, N.; Oveisi, E.; Loiudice, A.; De Gregorio, G. L.; Andreussi, O.; Marzari, N.; Buonsanti, R. Potential-Induced Nanoclustering of Metallic Catalysts during Electrochemical CO_2 Reduction. *Nat. Commun.* **2018**, *9*, 3117.

(48) Möller, T.; Scholten, F.; Thanh, T. N.; Sinev, I.; Timoshenko, J.; Wang, X.; Jovanov, Z.; Gliech, M.; Roldan Cuenya, B.; Varela, A. S.; Strasser, P. Electrocatalytic CO_2 Reduction on CuOx Nanocubes: Tracking the Evolution of Chemical State, Geometric Structure, and Catalytic Selectivity Using Operando Spectroscopy. *Angew. Chem., Int. Ed.* **2020**, *59*, 17974–17983.

(49) Kim, D.; Kley, C. S.; Li, Y.; Yang, P. Copper Nanoparticle Ensembles for Selective Electroreduction of CO_2 to C_2-C_3 Products. *Proc. Natl. Acad. Sci. U. S. A.* **2017**, *114*, 10560–10565.

(50) Mayyas, M.; Kalantar-Zadeh, K.; Mousavi, M.; Ghasemian, M. B.; Abbasi, R.; Li, H.;

Christoe, M. J.; Han, J.; Wang, Y.; Zhang, C.; Rahim, M. A.; Tang, J.; Yang, J.; Esrafilzadeh, D.; Jalili, R.; Allioux, F. M.; O'Mullane, A. P. Pulsing Liquid Alloys for Nanomaterials Synthesis. *ACS Nano* **2020**, *14*, 14070–14079.

(51) Song, M.; Mehrabian, N.; Karuturi, S.; Dickey, M. D. Jumping Liquid Metal Droplets Controlled Electrochemically. *Appl. Phys. Lett.* **2021**, *118*, 081601.

(52) Anderson, T. J.; Ansara, I. The Ga-Sn (Gallium-Tin) System. *J. Phase Equilibria* **1992**, *13*, 181–189.

(53) Pourbaix, M. *Atlas of Electrochemical Equilibria in Aqueous Solutions*, 2nd ed.; National Association of Corrosion Engineers: Houston, 1966.

(54) Popova, S.; Fomicheva, L. Crystallization of Tungsten-Gallium Alloys at High Pressure. *J. Less Common Met.* **1981**, *77*, 137–140.

(55) Parker, C. J.; Krishnamurthi, V.; Zuraiqi, K.; Nguyen, C. K.; Irfan, M.; Jabbar, F.; Yang, D.; Aukarasereenont, M. P.; Mayes, E. L. H.; Murdoch, B. J.; Elbourne, A.; Chiang, K.; Daeneke, T. Synthesis of Planet-Like Liquid Metal Nanodroplets with Promising Properties for Catalysis. *Adv. Funct. Mater.* **2023**, 2304248.